Journal of Applied Fluid Mechanics, Vol. 16, No. 7, pp. 1414-1426, 2023.
Available online at www.jafmonline.net, ISSN 1735-3572, EISSN 1735-3645.
https://doi.org/10.47176/jafm.16.07.1760

Numerical and Experimental Enhancement of the Aerodynamic Performance of a Road Vehicle using Passive Flow Control

C. Bayindirli

Nigde Vocational School of Technical Sciences, Nigde Omer Halisdemir University, Nigde, 51100, Turkey

Corresponding Author's Email: cbayindirli@ohu.edu.tr

(Received January 14, 2023; accepted March 1, 2023)

ABSTRACT

This study focused on reducing the drag force of a road vehicle using passive flow control. The aerodynamic performance of the model vehicle was improved by applying originally designed vortex generators. The drawing data of the model vehicle and vortex generators were designed in the Solid Works® program. The drag force measurements and flow visualizations were performed in the Fluent® program with the Reynolds numbers in the range of 2.8×10^5-6.6×10^5. Accordingly, the C_D value of the base model vehicle decreased by 6.22%, 4.59%, 3.38%, and 3.04%, respectively, using the originally designed vortex generator. This aerodynamic improvement rate can decrease the fuel consumption of vehicles by up to 3.3% at high vehicle speeds. To verify the highest numerical drag reduction, the model vehicle and vortex generators were produced in a 3-D printer. The vortex generators were mounted on the vehicle models with the lowest C_D value as in CFD analysis. The wind tunnel tests were conducted under the same test conditions for two vehicle models. It was determined that the experimental results supported numerical drag reduction.

Keywords: Aerodynamic; CFD; Drag coefficient; Vortex generator; Wind tunnel.

NOMENCLATURE

A	frontal area of the bus model
C_D	drag coefficient
F_D	drag force
u_∞	free stream velocity
Re	Reynolds number
ν	kinematic viscosity
CFD	Computational Fluid Dynamics
Exp.	experimental
AFC	Active Flow Control
PFC	Passive Flow Control
VG	Vortex Generator
IDDES	Improved Delayed Detached Eddy Simulation

1. INTRODUCTION

The aerodynamic parameters of a vehicle are very important in terms of fuel economy, especially at high speeds. Vehicles can continue their way in a balanced manner while on the road at high speeds if they have a good aerodynamic design. Aerodynamic science studies the interaction of rigid bodies with air during movement. A CFD method, road tests, and wind tunnel experiments are used to determine vehicles' aerodynamic properties. Although road tests may seem to be the most appropriate method for testing the vehicle due to the realistic environment, the cost of this method can be high. Since scaled models are used in wind tunnel tests, it is a cheaper method than models used in road tests. However, if the model's dimensions are increased or real-sized test models are used, wind tunnel testing may be costlier than road testing. Due to the cost of these methods, computerized analysis software has been widely used in recent years. This method can analyze even complex systems both cheaply and quickly. In this way, deficiencies and defects of the design can be determined in advance, and early measures can be taken while the design is yet in the production phase. Flow control methods are used to reduce aerodynamic drag forces acting on vehicles. Flow control is divided into two groups depending on the engine's energy consumption. PFC does not consume any energy from the vehicle, which makes PFC advantageous compared to active flow control. The literature summaries of the studies to increase vehicles' energy efficiency and reduce the drag force are presented below.

Altaf *et al.* (2022) applied PFC methods to a bus model and examined the effect on drag force using the computational fluid dynamics method. The researchers performed analyses in the Fluent program using the k-omega turbulence model. They achieved aerodynamic improvement with three different fin models in the shape of shark fins between the rates of 7.13-9.0%, with separator plates at 1.7%, with roughness plate on the vehicle surface at 2.32%, with various flow vent modifications up to 1.6%, and with passive air canals at 6.5%. Anantha and Rahul (2016) used PFC parts to decrease an SUV model's drag force and fuel consumption. Rear fairing, rear plate, delta-shaped wing and bump-shaped VG reduced drag between 6.5-26%. Delta-type wing vortex generators were more effective in drag reduction. The airflow features under the hood were investigated in CFD regarding drag. It was determined that manipulating the cooling airflow could provide lower drag and better radiator performance. PFC parts and modifications can improve the aerothermal performance of a vehicle (Zhang *et al.* 2018). Another study investigated the change in the vehicle's aerodynamic properties by adding PFC parts to a truck trailer vehicle. Four designs were developed as PFC equipment. In half-wing geometries of NACA 0009, NACA 0012 and NACA 0015 redirectors were added on top of the trailer. A conical tail was mounted on the rear of the trailer as an afterbody. A 17.8% aerodynamic reduction was achieved with the addition of a spoiler. When the half NACA airfoil was added in addition to the spoiler design, this improvement was 27.5%, whereas it was 28.5% with a conical tail (Kesat 2019). Yarin (2019) aerodynamically analyzed 5 vehicles using ANSYS Fluent software. The C_D value was found to be 0.74 in model 1 vehicle, in which excessive sharp corners and, accordingly, the deterioration of the flow on the vehicle occurred too much. C_D was decreased to 0.48 by eliminating sharp corners. By designing the vehicle model in the drop form, the C_D value was reduced to 0.27 by inclining the rear luggage section of the vehicle model, and the C_D value was 0.25. According to the analysis results, a significant decrease in C_D could be achieved by improving the regions with the flow deterioration. A high percentage of the fuel consumption of road vehicles is related to the aerodynamic drag force. It contributes up to 50% of the total vehicle fuel consumption at high speeds. Decreasing the aerodynamic drag provides an important solution to improving energy efficiency (Wood and Bauer 2003; Chilbule *et al.* 2014; Sudin *et al.* 2014). To this end, the C_D values of an SUV and a sedan vehicle were decreased by reducing the friction drag. The tapered smooth edges were used to decrease drag in an SUV model and a diffuser for a sedan car in order to obtain lower C_D values. The C_D value was reduced by 0.02 in the SUV model with smooth tapered edges at the rear end. In the sedan model, the C_D value was reduced from 0.33 to 0.29 using a diffuser (Nigal Ashik *et al.* 2020). Modifications, such as dimples, were investigated in a bus model using both CFD and a wind tunnel to decrease fuel consumption. The bus model was designed, and C_D was experimentally determined by wind tunnel tests. The dimple position, dimple number, and dimple orientation were tested to understand their effects on drag. It was stated that this method effectively decreased drag force and increased fuel economy for the bus model (Palanivendhan *et al.* 2021). The flow analysis of an SUV model was conducted in the study. The model vehicle was modified by attaching a lip kit to the front bumper. In comparison with the original model, the pressure increased by about 3.5%, the velocity by 3%, the lift force by 50.6%, and the drag by 5.8% in the modified SUV model (Yadav *et al.* 2021). The aerodynamic performance of a passenger car in the J segment and an SUV mode was numerically investigated in ANSYS Fluent software. The effects of reducing the windshield angle, rounding sharp lines on the vehicle model, and roofline slope on the C_D and lift C_L coefficients were calculated. After optimizations of the model's C_D value, which was 0.255, it was reduced up to 20%. Additionally, the C_L coefficient, which was -0.218, was reduced to 0.337. The maximum pressure value was reduced from 559.2 Pa to 536.5 Pa. As a result of the geometric optimizations, a more stable profile was obtained in the streamlines, and the areas where the speed vectors lost speed on the vehicle surface were reduced. Thus, the aerodynamic efficiency was improved (Kalaycı 2021). The flow analysis was carried out to determine the effects of trailing edge-integrated lobe-mixing geometries on the drag force of a truck trailer model in a study. Different lobe configurations of penetration angle and pitch values within $0.027< p/W <0.105$ and $5°<\beta<30°$, respectively, were investigated and compared to the base model. Side and top edges tapered with the optimum taper angle of a=15° reduced the drag force up to 10.8%. As a result, the lobed mixer configurations provided significant drag reductions that persisted with the increasing penetration angle up to β=30° (Rejniak and Gatto 2021). Synthetic jets and steady blowing were compared to determine their effects on drag reduction in an Ahmed body model. The experimental tests were conducted in a wind tunnel. The blockage ratio was approximately 10%. The C_D value of the Ahmed body with a rear slant angle of 25° was 0.333. The numerical flow analyses were carried out using LES. The difference between LES and the experiment was 1.8%. A 3% drag reduction was obtained using steady blowing, while a 9% drag reduction was achieved using synthetic jets. Compared to steady blowing, the results of optimal parameters for synthetic jets, which were installed between the roof and rear slant, showed higher drag reduction efficiency (Wenshi Cui *et al.* 2015). Bayindirli *et al.* (2020) developed four different spoilers for flow control on a bus model. They installed different distances to the bus in order to ensure drag force minimization. A drag reduction between 4.35–23.49% was obtained in the wind tunnel with different spoiler model applications. Another study experimentally investigated the excellent hydrodynamic features of tuna. Three types of bionic surfaces were designed and manufactured based on tuna skin. Its mechanical properties and construction were inspired and exemplified in the study. The features of the surface and coating of bionic surfaces were investigated, and

their effects on drag reduction performance were determined. The results showed that the drag reduction effects were proportional to the flexible coating thickness. A 7.22% drag reduction was achieved in the dual-structure coupling surface (Chen *et al.* 2022). According to Edwige *et al.* (2022), using jet devices as AFC is a promising approach for drag force affecting vehicles. CFD studies were performed around the Ahmed body model. Three actuation strategies were investigated at Re 500,000 based on the vehicle's height. The study showed that shear layer variations were formed during the blowing phase. The pulse/suction strategy reduced drag force by up to 8%. The change in flow topology occurs with synthetic jets and suction. Due to this, the rear back pressure advances substantially. The effect of the decreased aerodynamic drag coefficient on fuel consumption is observed under steady flow conditions in a passenger-type land vehicle with a mass of 1060 kg and a front surface area of 1.77 m^2. When the C_D value decreases from 0.5 to 0.3 at a constant driving speed of 96 km/h, a 23% improvement in fuel economy is achieved (Çağan 2000). This study aims to reduce a vehicle's aerodynamic drag and thus increase its energy efficiency. The vortex generator, which was originally designed, was placed on the vehicle's roof in four combinations. The effect of this PFC on the drag force was determined by the CFD method. The results of the CFD analysis were experimentally verified in the wind tunnel.

2. MATERIAL AND METHOD

In their study, Bayindirli and Çelik (2018) determined the flow structure and drag force of the base vehicle model. The sizes of the model vehicle were 11.83 cm in width, 15.18 cm in height, and 29.5 cm in length. In this study, multiple vortex generators were used as the PFC method. Figurs 1 and 2 show the drawing data of the vehicle model and vortex generators. After the CFD flow analysis of the base vehicle, it was seen that the flow separated in the roof area. Ten vortex generators were mounted in this area of the vehicle. By making the laminar flow turbulent, the flow's higher adherence to the surface delays the flow separation and improves the pressure-induced drag force. It is known that keeping the flow at the surface, delaying

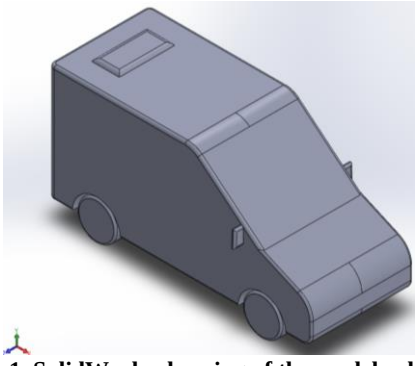

Fig. 1. SolidWorks drawing of the model vehicle (Bayindirli and Celik 2018).

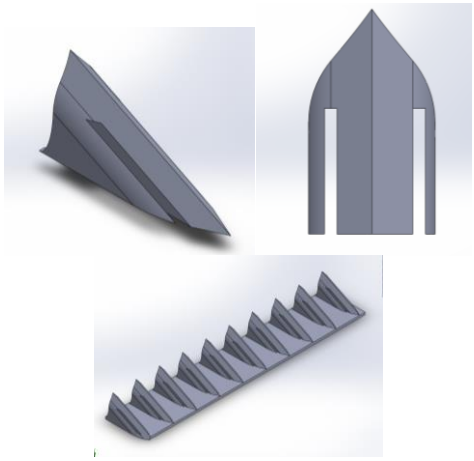

Fig. 2. Vortex generator's drawing.

flow separation, and reducing the negative pressure area will reduce the pressure-induced drag force (Yanqing *et al.* 2023). Thus, it was intended to reduce flow separation on the roof panel using multiple VG applications. The positions of the VG on the vehicle are given in Figs. 3-6.

It is important to verify CFD results with experimental results in studies on vehicle aerodynamics to ensure the reliability of results. In this study, two test model vehicles were experimentally investigated under the same test conditions to verify numerical drag reduction. As seen in Figs. 7 and 8, the produced vortex generators were mounted on the vehicle as in the CFD study.

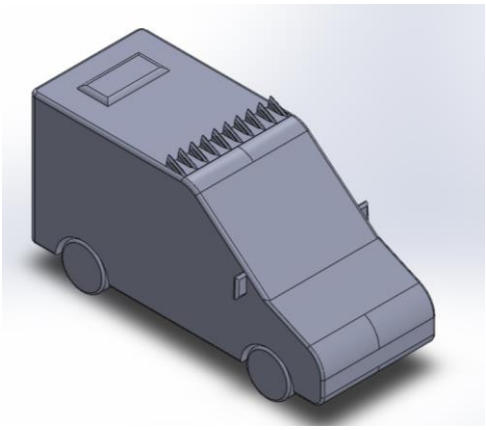

Fig. 3. Vortex generator application on model 1.

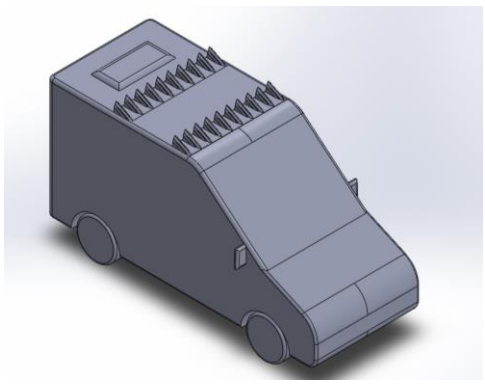

Fig. 4. Vortex generator application on model 2.

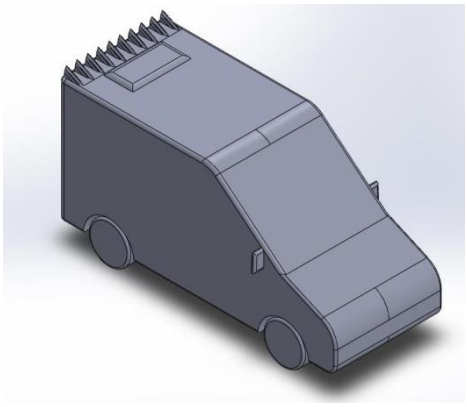

Fig. 5. Vortex generator application on model 3.

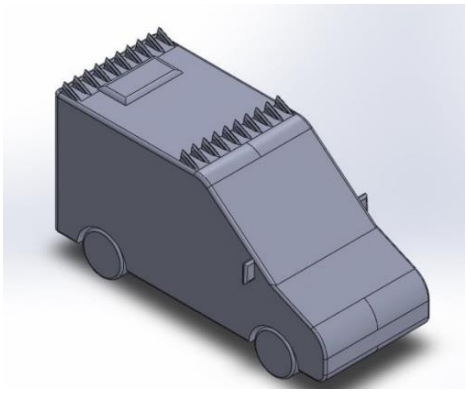

Fig. 6. Vortex generator application on model 4.

Fig. 7. Vortex generator application on model 1 (experimental).

Fig. 8. Vortex generator application on model 2 (experimental).

2.2. Similarity Conditions

Three similarity conditions (geometric, kinematic, and dynamic) must be provided between the model vehicle and prototype vehicle in aerodynamics studies. In this study, the model vehicle and VG were produced in a 3-D printer using the SolidWorks drawing data of the vehicle and vortex generator. Thus, the geometric similarity was provided. The blockage ratio should be lower than 7.5% to provide kinematic similarity in aerodynamic studies (Çengel and Cimbala 2008). The frontal area of the vehicle model was 0.01796 m^2, and the frontal surface area of the wind tunnel's test section was 0.3364 m^2. The rate of the frontal area of the vehicle model to the test section gives the blockage rate. It was 5.34% in the wind tunnel. To provide it in CFD analysis, the solution domain was created in the same dimensions. For the last similarity condition, Reynolds number independence was used to provide dynamic similarity, as generally employed in the literature.

2.3. CFD Algorithm

The numerical flow analysis was carried out in ANSYS Fluent® software using the k-ε RNG turbulence model due to processing time and being the most suitable turbulence model in terms of simplicity on a workstation computer (Kaya and Karagöz 2007). The sizes of the solution domain are 40x40x100 cm in the wind tunnel's test section. The model vehicle was positioned 15 cm from the inlet as in the wind tunnel. The turbulence intensity was 1%, the air density was 1 kg/m^3, the dynamic viscosity was 1.56x10-5 Pa.s, and the convergence criteria were 1.0×103. In CFD analysis, the flow was defined as a steady, incompressible, Newtonian fluid. The fluid-structure interaction, heat transfer effects, and body forces were neglected. The general integral equations of energy, momentum, continuity, and turbulence were solved in Fluent software using the finite volume method. The analyses were performed as a standard initialization using SIMPLE Least Squared Cell Based, standard wall functions, and segregated algorithm. It is difficult to analytically solve these equations. Therefore, packet programs are used to solve these equations numerically.

The continuity equation is expressed as the mass balance in a control volume in a flow (Ince 2010). For incompressible fluids, the density is constant, and the continuity equation is expressed in Eq. 1:

$$\frac{\partial u}{\partial x}+\frac{\partial v}{\partial y}+\frac{\partial w}{\partial z}=0 \quad (1)$$

The Navier–Stokes and continuity equations are also referred to as differential equations of motion. In solving these equations, three components (x, y, and z) of pressure and velocity are calculated by making some assumptions. Thus, it can be said that the Navier-Stokes equations are the dynamic expression of the balance of forces in any region of the given fluid, as in Eqs. 2-4. The most useful version of the Navier–Stokes equations for developing the finite volume method is presented below (Ince 2010):

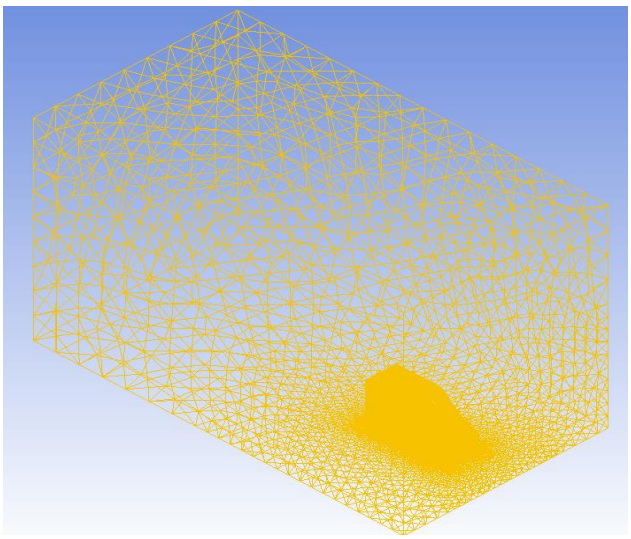

Fig. 9. Mesh distribution on model 1 solution domain area.

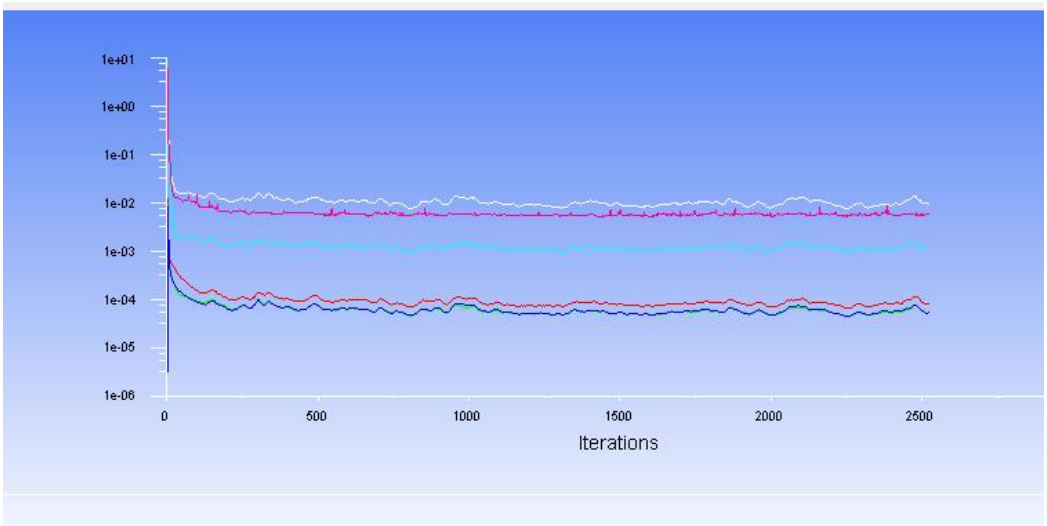

Fig. 10. Convergence graph in flow analysis.

$$\rho \frac{Du}{Dt} = -\frac{\partial p}{\partial x} + div(\mu gradu) + S_{M_x} \quad (2)$$

$$\rho \frac{Dv}{Dt} = -\frac{\partial p}{\partial y} + div(\mu gradv) + S_{My} \quad (3)$$

$$\rho \frac{Dw}{Dt} = -\frac{\partial p}{\partial z} + div(\mu gradw) + S_{Mz} \quad (4)$$

2.4. Mesh Strategy in CFD

A correct mesh distribution in the solution domain is of great importance for understanding the flow structure around the vehicle in detail and determining the true drag force.

As seen in Fig. 9, triangular unstructured tetrahedral meshes between the numbers 3152980-3282704 were formed in the solution domain. Proximity and curvature meshing were used after defining boundary conditions. The adaptive meshing method was used to obtain better mesh distribution and true solutions in numerical flow analyses. The method increases solution accuracy by making dynamic refinement.

The aerodynamic drag force was obtained, and C_D was calculated using Eq. 5:

$$C_D = \frac{F_D}{\frac{1}{2}\rho V^2 A} \quad (5)$$

2.5. Mesh Independence in CFD Analysis

In complex geometry, it is difficult to obtain high mesh quality due to curved and small parts. The desired mesh mostly could not be obtained in flow analysis. Therefore, mesh independence tests are performed in the aerodynamic analysis of model vehicles. As given in Fig. 11, mesh independence flow analyses were conducted in 8 various mesh counts at 567308 Re for model 1 vehicle.

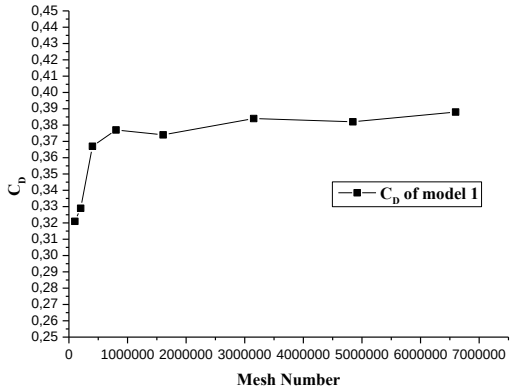

Fig. 11. Graph of mesh independence.

As seen in Fig. 11, the C_D coefficients were obtained at approximate values after a 1.6 million mesh count. The mesh count was 3043192 for model 1 and in the mesh independence region. Thus, it was accepted in studies that numerical tests were conducted independently of the mesh quality.

2.6. Wind Tunnel

The experiments were done in an absorption-type wind tunnel. The highest flow speed was 30 m/s, and the sizes of the test region were 400×400×1000 mm. The desired flow speed was provided by the fan motor in the test region. A frequency inverter controlled rpm. It had a 0.1 Hz step and a range of 0-50 Hz. The tests were conducted between 3.8×10^5–7.9×10^5 Re as in CFD analysis.

Figure 12 presents the experimental setup. Drag forces were measured by load cell with 0.1% accuracy in experimental studies. It can calculate force to 5 lb. The aerodynamic force measurements were made for 20 seconds. The sample was 1000 Hz for each test. To calculate the average drag force value, 20000 values were used for every test. A pitot tube was used to determine flow speed in the test section. A real-time multi-analyzer and external recorder were used in the studies. To read voltage outputs, data acquisition software was used.

2.7. Uncertainty analysis of experimental results

The uncertainties of the experimental setup determine the accuracy of experimental test results.

Fig. 12. Experimental setup.

Table 1 Uncertainty values of the calculated parameters (Bayindirli *et al.* 2020).

Calculated Parameter	Uncertainty value (%)
Reynolds Number	3.87
Drag force	4.5
Drag coefficient	4.7

Table 2 Base model C_D coefficients (Bayindirli and Celik 2018).

Velocity (m/s)	Re	C_D
15	2.8×10^3	0.435
20	3.7×10^3	0.433
25	4.7×10^3	0.391
30	5.6×10^3	0.412
35	6.6×10^3	0.405
	Average	0.415

Table 3 Comparison of C_D values of the base model – model 1.

Re Number	Base model C_D (CFD)	Model 1 C_D (CFD)	Reduction in C_D (CFD)
2.8×10^3	0.435	0.408	6.21%
3.7×10^3	0.433	0.398	8.08%
4.7×10^3	0.391	0.378	3.32%
5.6×10^3	0.412	0.384	6.8%
6.6×10^3	0.405	0.378	6.67%
Average	0.415	0.389	6.22%

Table 1 contains the uncertainty values of the calculated parameters.

3. NUMERICAL RESULTS IN CFD

3.1. Determination of the Base Model C_D

As given in Table 2 and Fig. 13, Bayindirli and Celik (2018) determined the C_D value of the base model vehicle as 0.415 at 5 different Re numbers. Additionally, they stated that the total drag force consists of 91.20% pressure base and 8.8% friction base.

3.2. Determination of Model 1 C_D

The C_D values of model vehicle 1 were determined as 0.389 at the same Re number. As shown in Table 3 and Fig. 13, the C_D value of the base vehicle was reduced by 6.22% using this VG on the front of the roof panel.

The flow analysis demonstrated that flow adhered more to the roof panel surface and flow separation was delayed using the VG. This decreased drag force and provided better aerodynamic performance. Figure 14 shows the flow images of model 1.

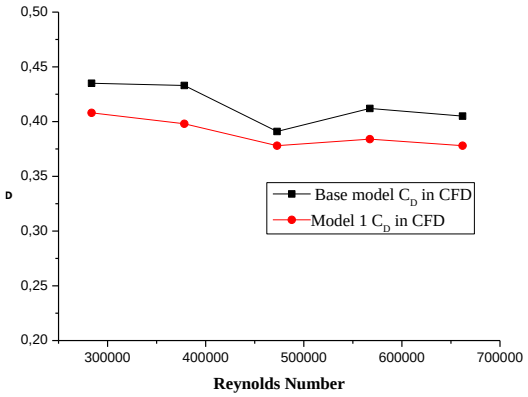

Fig. 13. Comparison graph of C_D values of the base model vehicle-model 1.

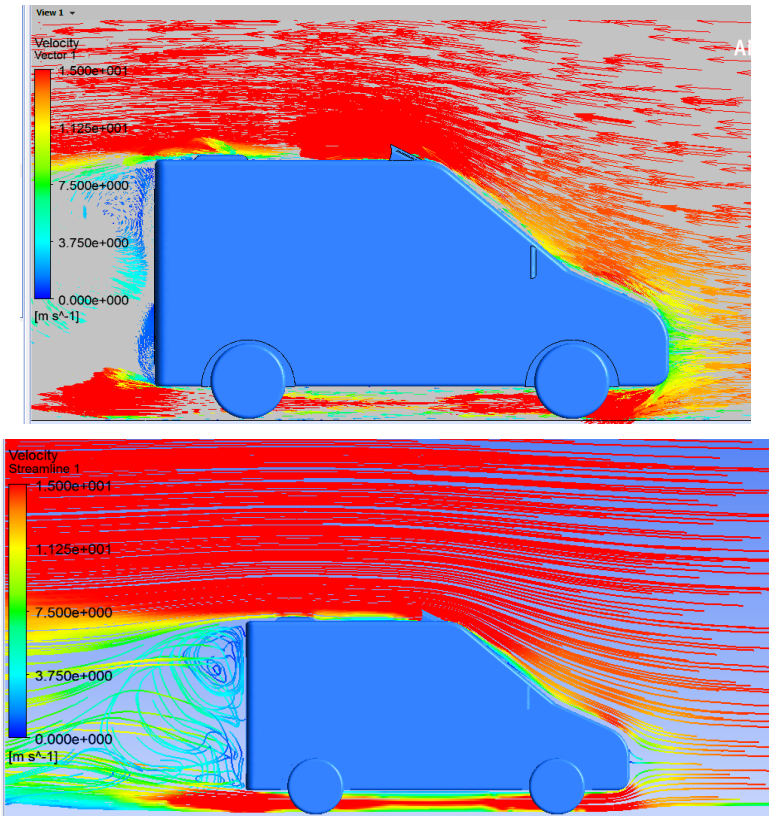

Fig. 14. Streamlines and velocity vectors on model 1 (15 m/s).

Table 4 Comparison of C_D values of the base model – model 2.

Re Number	Base model C_D (CFD)	Model 2 C_D (CFD)	Reduction in C_D (CFD)
2.8×10^3	0.435	0.423	2.76%
3.7×10^3	0.433	0.401	7.39%
4.7×10^3	0.391	0.376	3.84%
5.6×10^3	0.412	0.390	5.34%
6.6×10^3	0.405	0.394	2.67%
Average	0.415	0.397	4.59%

3.3. Determination of Model 2 C_D

In this study, two vortex generators were applied on the model vehicle, both at the front and middle of the roof panel. The C_D coefficient of the model vehicle was reduced by 4.59 % with the two-line vortex generator application, which was given in Table 4 and Fig. 15. Figure 16 presents flow visualization around model 3.

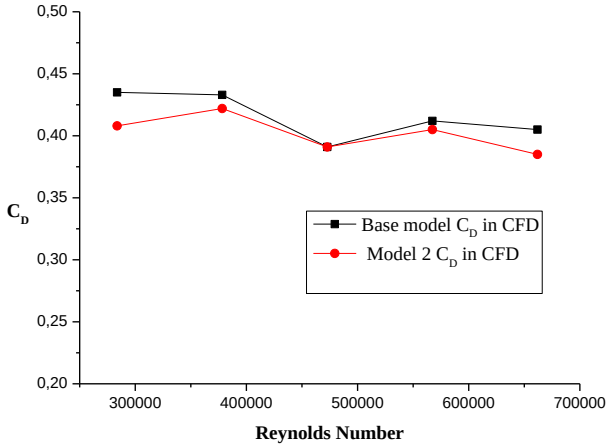

Fig. 15. Comparison graph of C_D values of the base model vehicle-model 2.

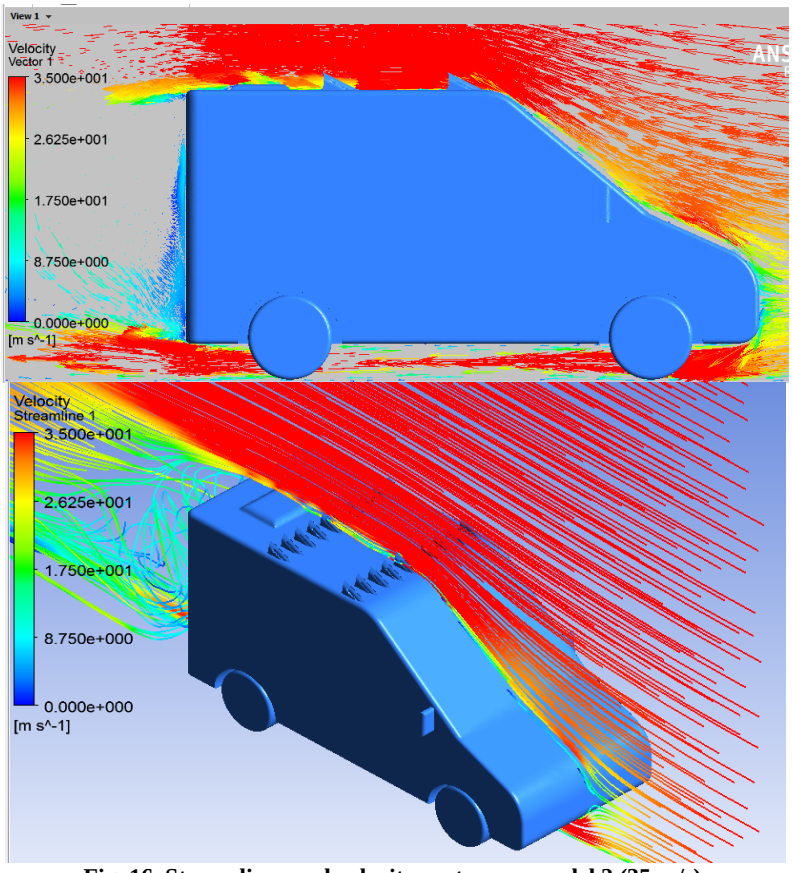

Fig. 16. Streamlines and velocity vectors on model 2 (35 m/s).

Table 5 Comparison of C_D values of the base model – model 3.

Re Number	Base model C_D (CFD)	Model 2 C_D (CFD)	Reduction in C_D (CFD)
2.8×10^3	0.435	0.408	1.96%
3.7×10^3	0.433	0.422	5.34%
4.7×10^3	0.391	0.391	2.68%
5.6×10^3	0.412	0.405	1.78%
6.6×10^3	0.405	0.385	5.13%
Average	0.415	0.402	3.38%

3.4. Determination of Model 3 C_D

In this model, the VG was mounted on the rear of the roof panel. According to the base model, an average 3.38% drag reduction was obtained. The C_D reduction rates for model 2 vehicle are presented in Table 5, the C_D graph is shown in Fig. 17, and the flow images of model 1 are given in Fig. 18.

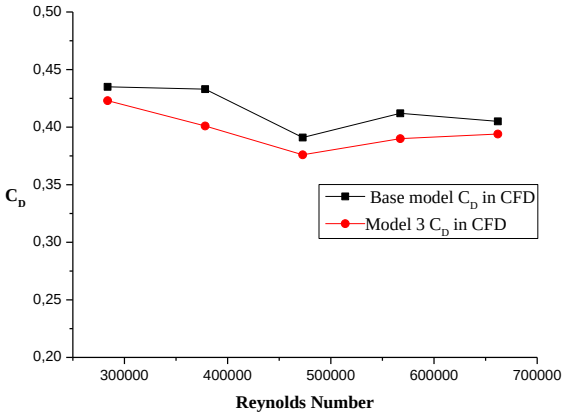

Fig. 17. Comparison graph of C_D values of the base model vehicle-model 3.

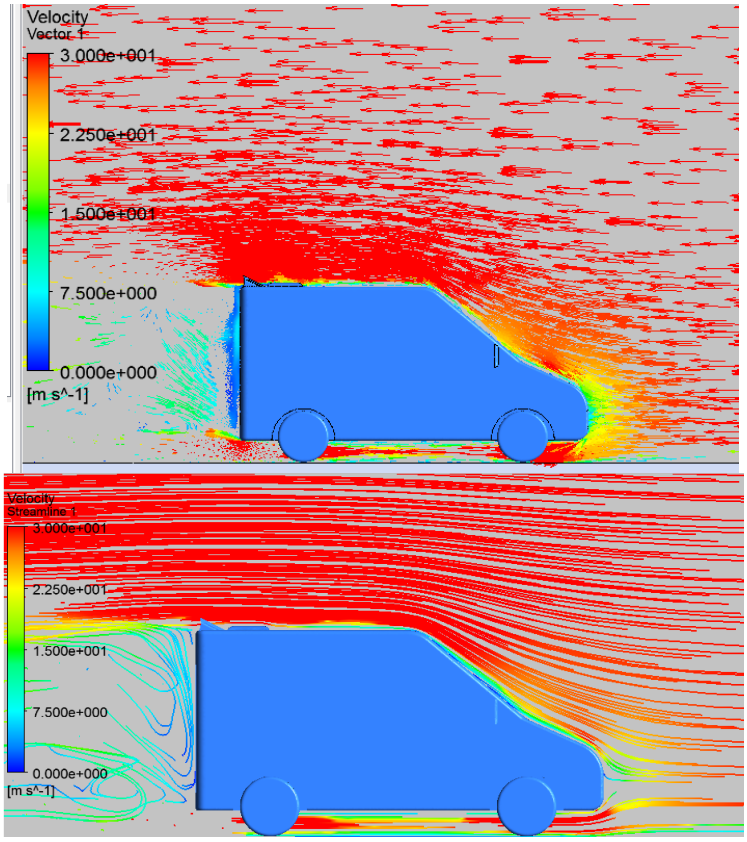

Fig. 18. Streamlines and velocity vectors on model 3 (30 m/s).

Table 6 Comparison of C_D values of the base model – model 4.

Re Number	Base model C_D (CFD)	Model 4 C_D (CFD)	Reduction in C_D (CFD)
2.8×10^3	0.435	0.414	5.17%
3.7×10^3	0.433	0.416	4.14%
4.7×10^3	0.391	0.391	0.13%
5.6×10^3	0.412	0.405	1.78%
6.6×10^3	0.405	0.389	4.01%
Average	0.415	0.403	3.04%

3.5. Determination of Model 4 C_D

Two vortex generators were applied on the model vehicle, both at the front and rear of the roof panel. The C_D value was decreased by 3.04%. The results of this application are given in Table 6 and Fig. 19. Flow visualization around model 4 is displayed in Fig. 20.

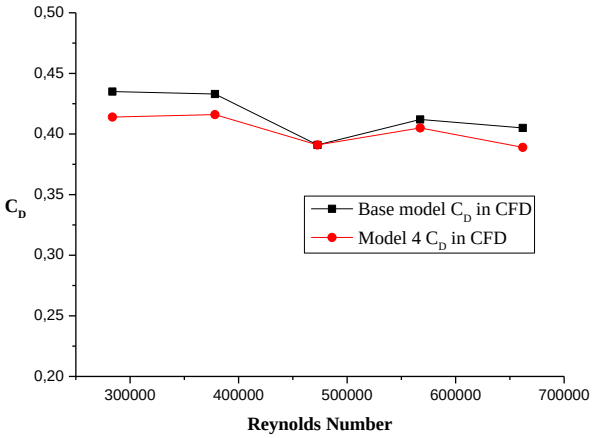

Fig. 19. Comparison graph of C_D values of the base model vehicle-model 4.

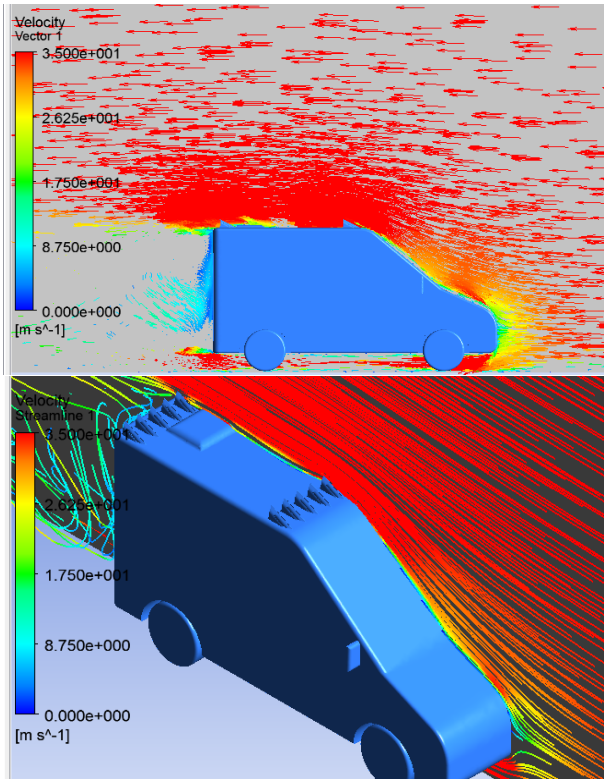

Fig. 20. Streamlines and velocity vectors on model 4 (35 m/s).

Flow separation in the rear windshield area causes the boundary layer to not adhere to the surface of the car body, expands and creates a big negative pressure area, which forms drag force (Palanivendhan *et al.* 2021). Vortex generators play a pivotal role in reducing drag and lift when placed at a specific distance upstream of the flow separation point. Moreover, coupling with a rear wing can give suitable downforce values and drag reduction by redirecting the air flow at the right angle of approach to the wing and preventing flow separation. The drag reduction can be obtained by changing the angle of attack of the airstream with the wing by changing the orientation of vortex generators (Kajiwara 2017). Likewise, in this study, a thin boundary layer was formed over the roof surface of the model vehicle, as seen in the CFD analysis of the base model. If the boundary layer length increases, the air flow moves away from the surface region. The flow separation occurs. This creates a negative pressure area, affecting vehicles on all surfaces. Furthermore, pressure-based drag force increases. By making the flow turbulent, it was kept more on the surface, flow separation was reduced, and the air flow was controlled in a thinner boundary layer using multiple VGs on the roof panel. Thus, the pressure-based drag force was improved by this PFC.

4. WIND TUNNEL TESTS

4.1. Validation of the Numerical Drag Reduction of Model 1

The wind tunnel tests were conducted at four free-stream velocities to verify the highest numerical drag reductions in model 1. The C_D value of the base

Table 7 Comparison of the experimental C_D values of the base model-model 1.

Re Number	Minibus C_D (Exp.)	Model 1 C_D (Exp.)	Reduction in C_D
266256	0.476	0.473	1.91%
345869	0.485	0.466	3.42%
434455	0.487	0.472	2.04%
528353	0.481	0.470	2.61%
Average	0.482	0.470	2.49%

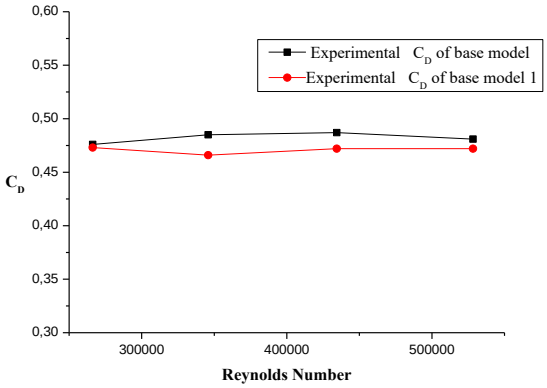

Fig. 21. Comparison graph of the experimental C_D values of the base model vehicle with model 1.

Table 8 Comparison of the experimental C_D values of the base model-model 2.

Re	Base model C_D (Exp.)	Model 2 C_D (Exp.)	Reduction in C_D
266220	0.476	0.473	1.91%
345812	0.485	0.473	1.82%
434406	0.487	0.478	0.78%
528302	0.481	0.473	1.90%
Average	0.482	0.474	1.60%

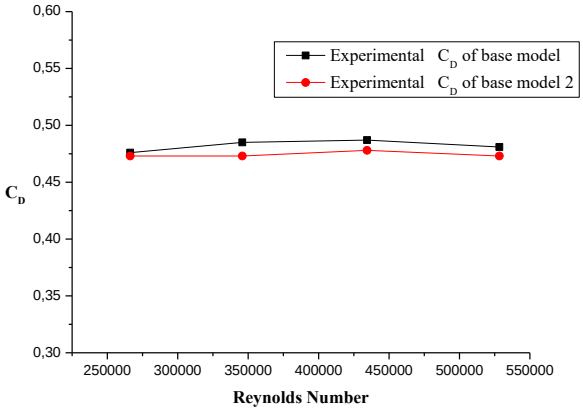

Fig. 22. Comparison graph of the experimental C_D values of the base model vehicle with model 2.

model vehicle was calculated as 0.482 in the wind tunnel. It was determined as 0.470 for model 1. As seen in Table 7 and Fig. 21, there was a 2.49% drag reduction according to the base model. The reduction rate was 6.22% in CFD. This experimental result supports the reduction in CFD. This difference between the experimental and CFD results may be due to the margin of error in the experimental setup, the uncertainty value, or the vibration in the wind tunnel.

4.2. Validation of the Numerical Drag Reduction of Model 2

As seen in Table 8 and Fig. 22, the C_D value of model 2 was determined as 0.474 in the wind tunnel. There was a 1.60% drag reduction according to the base model. The model vehicle and vortex generators

were 1/15 scaled to provide geometric similarity. The forces acting on this scaled model were quite small. CFD studies on small models can be conducted very sensitively. However, studying with small models in wind tunnels is difficult to detect the drag force reduction.

5. CONCLUSIONS

In this study, the C_D value of a 1/15-scaled model vehicle was improved by applying multiple VGs to the roof panel section. The numerical flow analysis was performed at 5 different free-flow velocities. The aerodynamic C_D value of model 1 was determined as 0.339 in CFD. The C_D value of the base model was 0.415. The 6.22% aerodynamic improvement was achieved using these VG applications. In model 2, to delay flow separation in the roof area of the vehicle, multiple vortex generators were mounted in both the front and middle areas of the roof panel. Thus, the C_D value of the base model decreased by 4.59% on average numerically. In model 3, to decrease the negative pressure area behind the model vehicle, a VG was mounted on the rear of the roof panel. The C_D value of the base model was decreased by 3.38%. In the last model, the VG was mounted both on the front and rear of the roof area, and a 3.04% drag reduction was obtained. To verify numerical drag reductions, the base model vehicle and vortex pairs were produced in the 3-D printer according to SolidWorks drawing data. The wind tunnel tests were conducted for the highest drag reductions. Model 1 and 2 vehicles were tested in the wind tunnel. A 2.49% drag reduction was obtained for model 1 and 1.60% for model 2. These experimental results verify numerical drag reductions with some margin fudge factor due to the uncertainty of test devices.

REFERENCES

Altaf, A., A. Omar and W. Asrar (2022). Passive drag reduction of the square back truck body. *International Journal of Automotive and Mechanical Engineering* 19-3, 9892- 9908.

Anantha, R. L. and H. H. Rahul (2016). Methods for reducing aerodynamic drag in vehicles and thus acquiring fuel economy. *Journal of Advanced Engineering Research* 3(1), 26-32.

ANSYS Fluent Tutorial Guide.pdf (https://forum.ansys.com/uploads/846/SCJEU0NN8IHX.pdf

Bayindirli, C., Y. E. Akansu and M. Celik (2020). Experimental and numerical studies on improvement of drag force of a bus model using different spoiler models. *International Journal Heavy Vehicle Systems* 27-6, 743-776.

Bayindirli, C. and M. Çelik (2018, 30 October-3 November). The investigation of flow structure around of a minibus model by CFD method. In *IV International Academic Research Congress*, 30 October-3 November, Alanya. Turkey.

Çağan, M. (2000). *Taşıt Aerodinamik Özelliklerinin Sayısal Yöntemlerle Incelenmesi*, M. Sc. thesis, Istanbul Technical University, Institute of Science and Technology: Istanbul.

Çengel, Y. A. and J. M. Cimbala (2008). *Fundamentals of fluid mechanics and applications.* Güven Bilimsel 562-599.

Chen, D., H. Chen and X. Cui (2022). Dual-coupling drag reduction inspired by tuna skin: Fan-shaped imbricated fish scale composited with flexible coating. *AIP Advances* 12, 035218.

Chilbule, C., A. Upadhyay and Y. Mukkamala (2014). Profile modification of truck-trailer to prune the aerodynamic drag and its repercussion on fuel consumption. *Procedia Engineering* 97, 1208-1219.

Edwige, S., P. Gilotte and I. Mortazavi (2022). Computational analysis of actuation techniques impact on the flow control around the ahmed body. *Fluids* 7, 52.

Ince, İ. T. (2010). *Aerodynamic Analysis of GTD Model Administrative Service Vehicle*. Ph. D. thesis, Gazi University Institute of Science, Ankara.

Kajiwara, S. (2017). Passive variable rear-wing aerodynamics of an open wheel racing car. Automot. *Automotive Engine Technology* 2(1-4), 107-117.

Kalaycı, C. (2021). *Numerical Investigation and Optimization of Aerodynamic Performance Of An Suv Model Motor Vehicle*. M. Sc. thesis, Institute Of Graduate Studıes Of Batman University.

Kaya, F. and İ. Karagöz (2007). Investigation into the suitability of turbulence models in swirling flows. *Uludağ Üniversitesi Mühendislik Fakültesi Dergisi* 12 (1) 85-96.

Kesat, T. M. (2019). *Çekici Römorke Etki Eden Aerodinamik Kuvvetler Üzerine Doğadan Esinlenerek Geliştirilen Pasif Akış Kontrol Parçalarının Etkilerinin İncelenmesi*. M. Sc. thesis, Karadeniz Teknik Üniversitesi Fen Bilimleri Enstitüsü.

Nigal Ashik, P. A., P. Suseendhar, N. Manoj and S. Wasim Feroze (2020). Reduction of drag in box-type and half streamlined automobile vehicles. *Materials Today: Proceedings*.

Palanivendhan, M., J. Chandradass, C. Saravanan, J. Philip and R. Sharan (2021). Reduction in aerodynamic drag acting on a commercial vehicle by using a dimpled surface. *Materials Today: Proceedings* 45, 7072-7078.

Rejniak, A. A. and A. Gatto (2021). On the drag reduction of road vehicles with trailing edge-integrated lobed mixers, *Proceedings of the Institution of Mechanical Engineers, Part D: Journal of Automobile Engineering, DOI: 10.1177/09544070211039697*

Sudin, M. N., M. A. Abdullah, S. A. Shamsuddin, F. R. Ramli and M. M. Tahir (2014). Review of research on aerodynamic drag reduction methods. *International Journal of Mechanical and Mechatronics Engineering IJMME-IJENS* 14-2, 35-45.

Wenshi Cui, W., H. Zhu, C. Xia and Z. Yang (2015). Comparison of steady blowing and synthetic jets for aerodynamic drag reduction of a simplified vehicle. *Procedia Engineering* 126, 388-392.

Wood, R. M. and S. X. S. Bauer (2003). Simple and low-cost aerodynamic drag reduction devices for tractor-trailer trucks. *SAE Technical Paper* 01(3377), 1-18.

Yadav, R., A. Islam and R. Chaturvedi (2021). Efficient reduction of the consumption of fuel in road vehicles using aerodynamic behavior in CDF analysis. *Materials Today: Proceedings* 45, 2773-2776

Yanqing, W., W. Ding, W. Yuju, M. Yuan, C. Lei and W. Jiadao (2023). Aerodynamic drag reduction on speed skating helmet by surface structures. *Applied Sciences* 13, 130.

Yarin, T. G. (2019). *Farklı Taşıt Modellerinin Aerodinamik Yapısının Nümerik Olarak İncelenmesi*. M. Sc. thesis, Bursa Uludağ Üniversitesi Fen Bilimleri Enstitüsü.

Zhang, L., M. Yang and X. Liang (2018). Experimental study on the effect of wind angles on pressure distribution of train streamlined zone and train aerodynamic forces, *Journal of Wind Engineering and Industrial Aerodynamics* 174, 330-343.